Polarization-entangled mid-infrared photon generation in p-doped semiconductor quantum wells

RAZALI, Razif, IKONIC, Zoran, INDJIN, Dragan and HARRISON, Paul <http://orcid.org/0000-0001-6117-0896>

Polarization-entangled mid-infrared photon generation in p-doped semiconductor quantum wells

R Razali[*1,3], **Z. Ikonić**[1], **D. Indjin**[1] **and P. Harrison**[2]

[1] School of Electronic and Electrical Engineering, University of Leeds, Woodhouse Lane, Leeds LS2 9JT, United Kingdom
[2] Materials and Engineering Research Institute, Sheffield Hallam University, Howard Street, Sheffield, South Yorkshire S1 1WB, United Kingdom
[3] Physics Department, Faculty of Science, Universiti Teknologi Malaysia, 81310, Skudai, Johor, Malaysia

E-mail: elrbr@leeds.ac.uk, razifrazali@utm.my

Abstract. The optimal design of double quantum well structures for generation of polarization-entangled photons in the mid-infrared range, based on the valence intersubband transitions spontaneous parametric downconversion, is considered. The efficiency and frequency selectivity of the process are also estimated.

PACS numbers: 1315, 9440T
Keywords: optimised quantum well, SPDC, nonlinear optics, entangled twin photons

Submitted to: *Semicond. Sci. Technol.*

1. Introduction

Quantum correlated photon pairs, also known as entangled photon pairs, are the main ingredient in quantum communications [1], quantum computing [1–3], quantum key distribution (QKD) [4], quantum teleportation [5], superdense coding [6] and many other applications of quantum information theory. These photon pairs can be generated in spontaneous parametric down conversion (SPDC), or in spontaneous four wave mixing (SFWM) [7]. SPDC, which is also known as parametric fluorescence [8], is based on second order nonlinearity ($\chi^{(2)}$), while SFWM is based on third order nonlinearity ($\chi^{(3)}$). Raman scattering noise, which is hard to suppress in SFWM [9], has made the SPDC scheme more attractive. The SPDC and SWFM processes, producing entangled photon pairs, can be induced in different media, like bulk crystals (possibly with tailored inhomogeneous nonlinearity [10]), quantum well heterostructures, in quantum dots [11, 12], or NV centres in diamond [13].

This work focuses on SPDC process based on intersubband transitions in the valence band of quantum well heterostructures. The incentive to consider this case comes from the fact that SPDC based on intersubband transitions within the conduction band Γ-valley (the most frequent case) does not provide polarization entanglement, since these transitions are active only for Z-polarization of light (perpendicular to the well layer)[14]. In contrast, valence band intersubband transitions are active for various polarizations, which comes from their *p*-like, rather than *s*-like character, enabling polarization entanglement in the SPDC process (in particular, the type II SPDC). Unlike the case of conduction band intersubband transitions, the optical parameters of valence band intersubband transitions cannot be calculated by the effective mass method, but rather by $\mathbf{k}\cdot\mathbf{p}$ method (in particular, for structures based on wider band gap materials, assumed in this work, the 6-band $\mathbf{k}\cdot\mathbf{p}$ method is sufficiently accurate). As for the structure design and optimisation, the methodology employer here is similar to what we have used previously [14]

As pointed in [15], which considered the optimization of the second harmonic generation (SHG) in p-type GaAs-AlAs step quantum well structures, the symmetry of hole state wavefunctions enables only 5 non-zero components of the second-order polarizability: ZXY, ZXX, XYZ, XXZ and ZZZ, where the first component denotes the generated SHG photon polarization, the other two being the pump photons. SPDC is similar to SHG, but reversed in time, so these selection rules apply to SPDC as well. Therefore, generation of polarization-entangled twin photons can rely on ZXY, XYZ or XXZ configuration. Practical considerations, suggesting that SPDC will be used in waveguide layout (co-propagating waves), imply that polarizations of the three waves cannot be all different, hence only the XXZ polarization will be considered here.

2. SPDC based on valence intersubband transitions

SPDC is a second order optical process, with the nonlinear polarization

$$\mathbf{P} = \epsilon_0 \chi^{(2)} \mathbf{E}^2 \tag{1}$$

determined by the second-order nonlinear susceptibility $\chi^{(2)}$ as given e.g. in [16, p. 174]. For intersubband transitions involving hole states in quantum wells the state energies $E_l(k_x, k_y)$ depend on their quantum index l and the in-plane wave vector (k_x, k_y), and the transition matrix elements also depend on (k_x, k_y), so the summation over all states, discretised in the (k_x, k_y) plane, is written as

$$\chi^{(2)}\left(\omega_p+\omega_q,\omega_p,\omega_q\right) = \frac{e^3 \Delta k_x \Delta k_y}{8\pi^2 L_z \epsilon_0 \hbar^2} \times$$
$$\sum_{k_x,k_y}\sum_{lmn}\left[f_{\mathrm{FD}}(E_l(k_x,k_y),E_F) - f_{\mathrm{FD}}(E_m(k_x,k_y),E_F)\right]$$
$$\left\{\frac{d^x_{ln} d^x_{nm} d^z_{ml}}{\left[(\omega_{nl}-\omega_p-\omega_q)-i\Gamma_{nl}\right]\left[(\omega_{ml}-\omega_p)-i\Gamma_{ml}\right]}\right.$$
$$+\frac{d^x_{ln} d^z_{nm} d^x_{ml}}{\left[(\omega_{nl}-\omega_p-\omega_q)-i\Gamma_{nl}\right]\left[(\omega_{ml}-\omega_q)-i\Gamma_{ml}\right]}$$
$$+\frac{d^x_{ln} d^x_{nm} d^z_{ml}}{\left[(\omega_{nm}+\omega_p+\omega_q)+i\Gamma_{nm}\right]\left[(\omega_{ml}-\omega_p)-i\Gamma_{ml}\right]}$$
$$\left.+\frac{d^z_{ln} d^x_{nm} d^x_{ml}}{\left[(\omega_{nm}+\omega_p+\omega_q)+i\Gamma_{nm}\right]\left[(\omega_{ml}-\omega_q)-i\Gamma_{ml}\right]}\right\}, \tag{2}$$

where e is the electron charge, Δk_x and Δk_y are the mesh steps in x- and y-directions, L_z is the total length of the structure in z-direction, ϵ_0 is the free space permittivity, ω_p, ω_q and $\omega_p+\omega_q$ are the frequencies of three photons interacting in the nonlinear system, and $\hbar\omega_{nm} = E_n(k_x,k_y) - E_m(k_x,k_y)$ is the subband spacing at a particular (k_x, k_y). In the SPDC case, ω_p and ω_q may denote the signal and idler photons, while $\omega_p+\omega_q$ is the pump photon that will be down-converted in the SPDC process. Γ_{ij} is the linewidth of $i \to j$ transition, and d^x_{ij} is the x-component of dipole matrix element for this transition. The state energies $E_m(k_x,k_y)$ and the matrix elements d^x_{ij} were calculated using 6×6 k.p method [17, p. 407].

The state populations in (2) are given by the Fermi-Dirac function f_{FD}:

$$f_{\mathrm{FD}}(E_a(k_x,k_y),E_F) = \left[1+\mathrm{e}^{\left(\frac{E_a(kx,ky)-E_F}{kT}\right)}\right]^{-1}. \tag{3}$$

where E_F is the Fermi energy in the structure, k is the Boltzman's constant and T is the temperature.

3. Degenerate Twin Photon Generation

Quantitative analysis of twin-photon generation in the presence of optical losses [18] shows that the degenerate twin photon generation is given by

$$P_{\text{Twin}} = \frac{4|\kappa|^2 P_3 L^{3/2}}{3\sqrt{2\pi|g|}} \frac{3e^{-|\alpha_{123}|L}}{2|\alpha_{12-3}L|^{3/2}} \times \int_0^{\sqrt{|\alpha_{12-3}L|}} \sinh(|\alpha_{12-3}L| - x^2)\, dx\ . \quad (4)$$

where $\alpha_{123} = \alpha_1 + \alpha_2 + \alpha_3$, $\alpha_{12-3} = \alpha_1 + \alpha_2 - \alpha_3$, $g = [\partial^2\beta/\partial\omega^2]$, and $\beta = 2\pi n_1/\lambda_1$. The α_i in (4) is the absorption coefficient at photon frequency ω_i, L is the length of the device, P_3 is the pump power, and κ is related to $\chi^{(2)}$ via

$$\kappa = \varepsilon_0 d_{\text{eff}} \sqrt{\frac{2\omega_1\omega_2}{n_1 n_2 n_3 S_{\text{eff}}} \left(\frac{\mu_0}{\varepsilon_0}\right)^{\frac{3}{2}}} \quad (5)$$

where $d_{\text{eff}} = 0.5\chi^{(2)}$, S_{eff} is the pump beam cross section. It should be noted that the three waves (1,2,3) each have generally different absorption coefficients α_i, either because of their frequency (pump vs. signal/idler) or because of their polarization (signal vs. idler, which are degenerate in frequency, but not in polarization). The n_i in Eqs.(4) and (5) is the refractive index at frequency ω_i, calculated from Sellmeyer's equation for GaAs and AlGaAs [19], including the temperature dependence [20], and then using the weighted average of the refractive indices for the constituent binaries in the structure (this is justified because the wavelengths involved are far larger than any layer thickness in the structure).

The absorption coefficient α in (4) is calculated from the imaginary part of linear susceptibility ($\chi^{(1)}$), as [16, p. 167]

$$\alpha = \chi^{(1)\prime\prime}\omega/c\ , \quad (6)$$

where $\chi^{(1)\prime\prime}$ is calculated as

$$\chi^{(1)\prime\prime} = \frac{\Delta k_x \Delta k_y}{(2\pi)^2 L_z} \frac{e^2}{3\hbar\epsilon_0} \sum_{k_x,k_y} \sum_n \{f_{\text{FD}}(E_l(k_x,k_y), E_F) - f_{\text{FD}}(E_m(k_x,k_y), E_F)\} |d^i_{lm}|^2 \times \left[\frac{\Gamma_{lm}}{\Gamma_{lm}^2 + (\omega_{lm} - \omega)^2} - \frac{\Gamma_{lm}}{\Gamma_{lm}^2 + (\omega + \omega_{lm})^2}\right]. \quad (7)$$

For resonant structures the absorption peaks at pump and signal / idler photon energies, just as the nonlinear susceptibility does, and must be accounted for.

As illustrated in Figs. 1(a) and 1(b), the product of dipole matrix elements depends on (k_x, k_y), but the pattern is replicated in each quarter of the k_x–k_y plane, which is used in summation over k_x, k_y points in Eq.(2) to speed up the calculations by a factor of 4, which is important for the optimisation process. In calculating $\chi^{(2)}$ the summation should include all k-points which

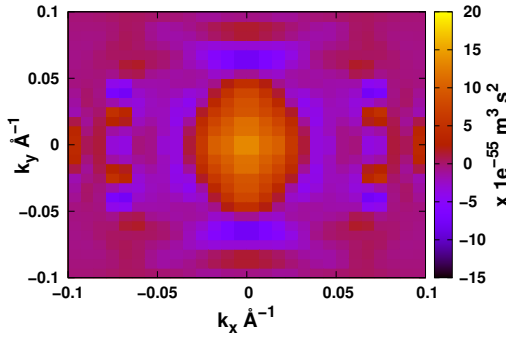

(a) Real part

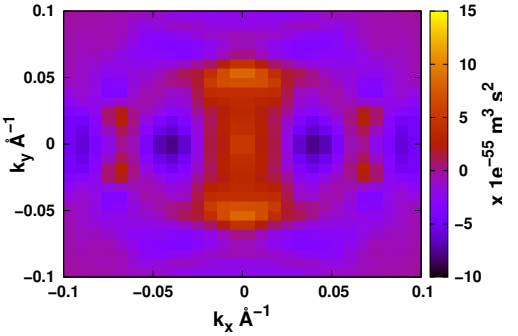

(b) Imaginary part

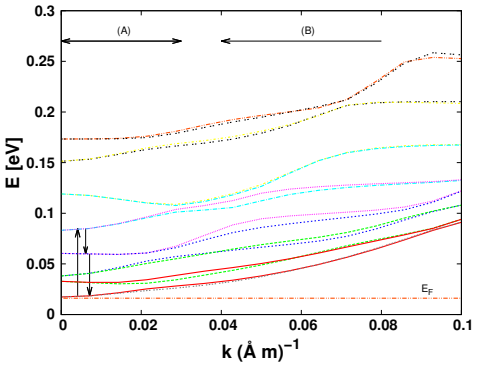

(c) The dispersion of quantised states

Figure 1: (a,b) The value of the $\{\ldots\}$ term in Eq.(2), calculated for the first structure from Table 1, as it depends on (k_x, k_y) and (c) The dispersion of quantised states in this structure, with the transition which, although off-resonant, gives the largest contribution to $\chi^{(2)}$ denoted (however, various other transitions also contribute significantly). The small (A) and large (B) wave vector ranges give opposite-in-sign contributions to $\chi^{(2)}$).

may have any significant population of holes, and with the in-plane dispersion of hole state varying from one structure to another: 10% of the Brillouin zone was taken as a safe limit. The number of k-points within this range is taken as 15 in each direction, which gives a reasonable convergence of the calculated value of $\chi^{(2)}$. In numerical calculations the pump power $P_3 = 1$ kW, and cross section $S_{\text{eff}} = 100 \times 100\ \mu m^2$ were used for reference.

Fig. 1 shows an example of the variation of the $\{\ldots\}$ term in (2) (product of matrix elements and resonance terms in denominators, but without the hole density-dependent Fermi-Dirac terms), as it varies across the (k_x, k_y) plane.

4. Optimization of SPDC efficiency

Quantum well structures suitable for SPDC were designed by performing a genetic optimization, with SPDC efficiency as the target. We consider the degenerate SPDC, with signal and idler photon energies fixed to 100 meV and the pump to 200 meV, while the linewidth Γ was assumed to have the 'typical' value of 10 meV for all transitions. Non-zero $\chi^{(2)}$ requires asymmetric quantum wells, and the simplest structures of this type are double quantum wells (DQW) and step quantum wells. The DQW structure with equally deep wells was chosen, because it can be more easily fabricated with good accuracy. Even for the technologically well developed AlGaAs system, the variable-width rectangular profiled structures (with just two different material compositions) can presently be grown with better accuracy than the variable-composition structures (even the simplest among them, the stepped quantum wells). They are the only type of heterostructures practically used nowdays for intersubband devices, e.g. in complex devices like quantum cascade lasers, despite the fact that an even better performance could sometimes idealistically be expected from carefully tailored variable-composition structures. The parameters to be varied are the widths of the two wells and the barrier, and the well depth is taken constant, determined by the material composition. The holes density is kept low (3.2×10^6 cm^{-2}) so that space charge potential could be neglected. The method of optimization is similar to that described in [14], the only difference being that we have chosen here the SPDC efficiency, rather than the value of $\chi^{(2)}$, as the target, so the effects of pump and signal/idler absorption are included.

The material system considered in this work is the technologically most developed AlGaAs alloy, with GaAs taken as the well and AlGaAs as the barrier material, with the Al content in the alloy equal to 48%. In Table 1, the structural unit is AlGaAs/GaAs/AlGaAs/GaAs/AlGaAs double quantum well (DQW), with the first and last layers being thick AlGaAs barriers, their thickness being somewhat arbitrarily set to 100 Angstrom ($\mathring{A}$) to make neighbouring DQWs independent, i.e. well isolated from each other. The widths of the three inner layers, coming from the optimisation procedure, are also given in Table 1 in $\mathring{A}$ units.

Table 1: The partially or fully optimized DQW structures, their SPDC efficiency, and the value of $\chi^{(2)}$, respectively.

structure	**SPDC efficiency**	$\chi^{(2)}$ **(m/V)**
100/34/5/76/100	2.11×10^{-21}	1.09×10^{-13}
100/36/12/62/100	1.31×10^{-21}	1.22×10^{-12}
100/82/5/24/100	3.88×10^{-22}	9.87×10^{-14}
100/13/18/54/100	3.18×10^{-22}	5.46×10^{-14}
100/40/9/68/100	3.03×10^{-22}	1.81×10^{-13}
100/68/9/40/100	2.64×10^{-22}	1.67×10^{-13}
100/11/58/49/100	1.11×10^{-22}	2.72×10^{-14}
100/55/29/81/100	2.77×10^{-22}	5.24×10^{-14}

Table 1 shows a number of best daughter structures, coming from different parents, retained before selecting the best one at the end of the optimisation procedure. This illustrates a limited correlation between nonlinear susceptibility and conversion efficiency, and in particular the fact that the highest value of $\chi^{(2)}$ does not imply that this structure will deliver the highest efficiency. The reason behind this is the absorption, as will be discussed in more detail in Sec. 5.

5. Effect of Holes Density on the SPDC Efficiency

In this section we consider the effect of the hole density, while keeping the interaction length limited to 100μm, on the SPDC efficiency. The holes density was varied from 5×10^6 to 2×10^{12} cm^{-2}, and the best (fully optimised) structure from Table 1 was used. As shown in Fig. 2(a), there exists an optimum density, for which the SPDC efficiency is largest. The reason behind this is that, as shown in Fig. 1, there are areas in the (k_x, k_y) plane where the relevant combination of dipole matrix elements has very high values. At low temperatures (T=77K) holes populate almost fully all the (k_x, k_y) states below the Fermi level, and states above it are almost empty. Increasing the hole density increases the Fermi level, and expands the range of (k_x, k_y) states which are populated. The value of $\chi^{(2)}$ then increases, because all the small (k_x, k_y) states have significant (and same sign) contributions to $\chi^{(2)}$, as shown in Fig. 1. However, adding even more holes does not necessarily mean that $\chi^{(2)}$ will steadily increase. There is an area in the (k_x, k_y)

plane where the {...} term in Eq.(2) changes sign, (Figs. 1(a),(b) and (c)) , and if this becomes populated with holes, the value of $\chi^{(2)}$ will actually decrease, as displayed in Fig. 2(b) (point after the optimum holes density). In addition, more holes will also increase the absorption (which only gets positive contributions from any (k_x, k_y)), as can be seen from Figs. 2(c)-(e), hence decreasing the SPDC efficiency. Therefore, choosing the correct value of holes density is important for achieving the highest SPDC efficiency, Fig. 2(a).

As shown in Fig. 2(c), the optimum interaction length L is always small for reasonably large values of hole density, across the temperature range of practical interest. Noteworthy, the coherence length l_c for this degenerate SPDC case is 1500 μm, as calculated from Sellmeyer's equation [19], and this value is applicable to large cross-section ('bulk-like') MQW structures. For L comparable to l_c the effective $\chi^{(2)}$ would decrease, and would even become very small if $L >> l_c$. However, employing quasi-phase-matching schemes would enable just a moderate reduction of l_c (by a factor of $2/\pi$) [21]. Alternatively, dispersion engineering (e.g. by dispersion engineering of the waveguide structure, to give the same velocity of pump and signal waves) would increase l_c itself. To avoid going into details on this side, we have used Eq.(4) in calculations, having in mind that some further reduction of efficiency might take place in real structures if the interaction length is large.

6. Effect of Pump Frequency Variation on the SPDC Efficiency

It is interesting to explore how 'broadband' a particular structure can be considered to be, so we next consider the effects of variation of the pump frequency around the value a particular structure is designed / optimised for (200 meV), on the SPDC efficiency. We take the optimum structure (100/34/5/76/100), at 77K and 300K, and choose the optimal values of hole densities and interaction lengths (extracted from Fig. 2(c), and given in Table 2), which deliver the peak efficiency at the design pump frequency, Fig. 2(a). The SPDC efficiency is then calculated for a range of pump photon energies, from 160 to 240 meV (while the signal and idler photon energies are always kept to a half of that value). The results are shown in Fig. 3.

As shown in Figs. 3(a), the structure optimised for 200 meV pump, with a low value of hole density, gives at 77K the highest efficiency for the pump energy at 205 meV (with the signal/idler at 102.5 meV), while at 300K its efficiency is highest for 210 meV pump (with signal/idler at 110 meV). However, these peak efficiencies are only slightly higher than for 200 meV pump. In fact, in this optimal structure

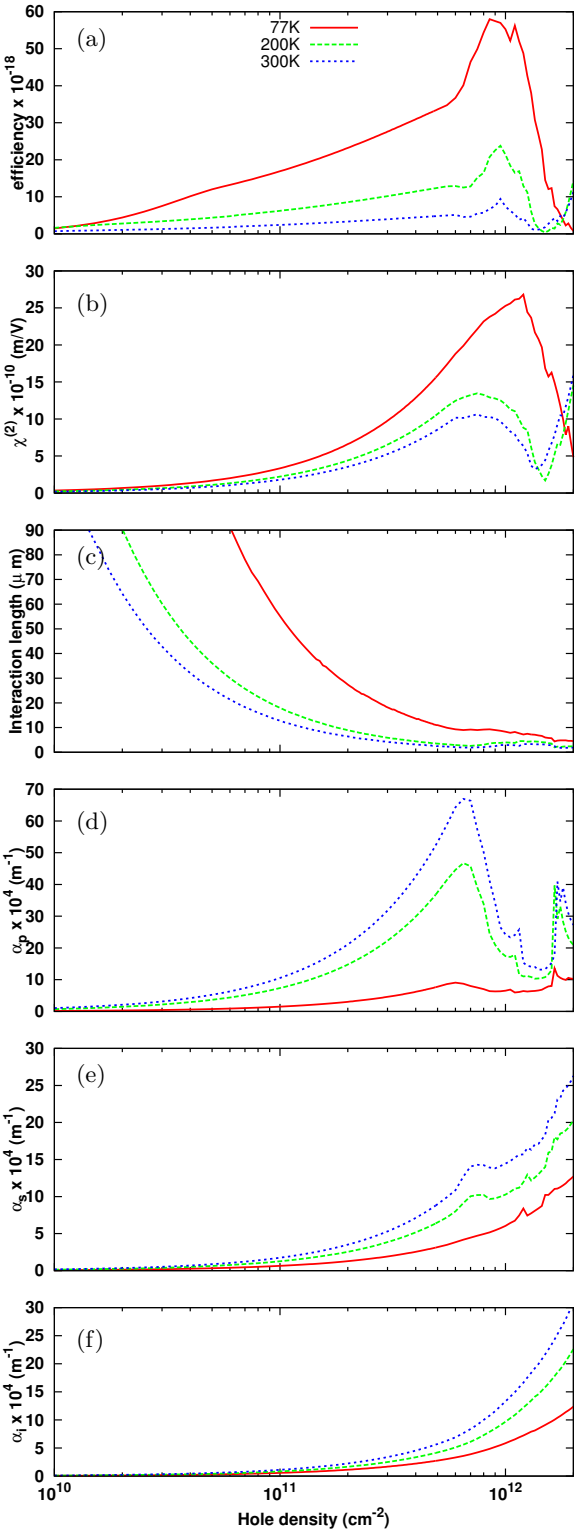

Figure 2: The hole density dependence of relevant parameters in the fully optimised structure at different temperatures: (a) conversion ratio, (b) $\chi^{(2)}$, (c) optimal interaction length, (d)-(e) the absorption coefficient for the pump, signal and idler wave (note that the signal and idler have the same frequency but different polarization). The solid red line in Fig. 2(a) is scaled down by 0.2, so that all lines are clearly visible

.

Table 2: The optimal values of hole density and interaction length for the structure (100/34/5/76/100), at different temperatures.

T (K)	Optim. hole density (cm^{-2})	L (μm)
77	8.5×10^{11}	9.3
200	9.5×10^{11}	3.8
300	1.0×10^{12}	2.9

neither the nonlinear susceptibility nor the absorption have any prominent resonant features, Figs. 3(b)-(e). Although $\chi^{(2)}$ decreases with increasing pump energy, the efficiency is still somewhat better in the higher energy range (200-240 meV) than in the lower energy range (160-200 meV), Fig. 3(a), because the absorption behaves in the opposite manner, and the resulting efficiency comes from the interplay of the two. Generally, the structure has a rather large useful bandwidth for SPDC, of ~ 40 meV, before its efficiency drops to a half of its peak value. This feature makes these devices perspective for communication systems.

It is interesting to note that the values of the conversion efficiency, Fig.3, depend quite strongly on temperature, but the position of the peak (and also its width) depend rather weakly on temperature. This comes from the fact that the general shape (frequency dependence) of nonlinear susceptibility and absorption coefficients of the three waves, Fig.3(b-e), does not change much with temperature, and the conversion efficiency, which depends on all these effects, inherits the temperature insensitivity of its frequency dependence (however the actual values of efficiency, on or off peak, are affected).

7. Conclusion

Optimization of p-doped quantum well structures to deliver efficient polarization-entangled twin-photon generation by spontaneous parametric down-conversion in the mid-infrared spectral range was performed using a genetic algorithm. Calculations show that the optimal structure lengths are rather small, with practically accessible levels of hole densities, and have a reasonably large bandwidth, which makes them practically interesting.

8. Acknowledgements

RR is grateful to the Ministry of Higher Education Malaysia and Universiti Teknologi Malaysia for providing financial support through the SLAB/SLAI Scholarship.

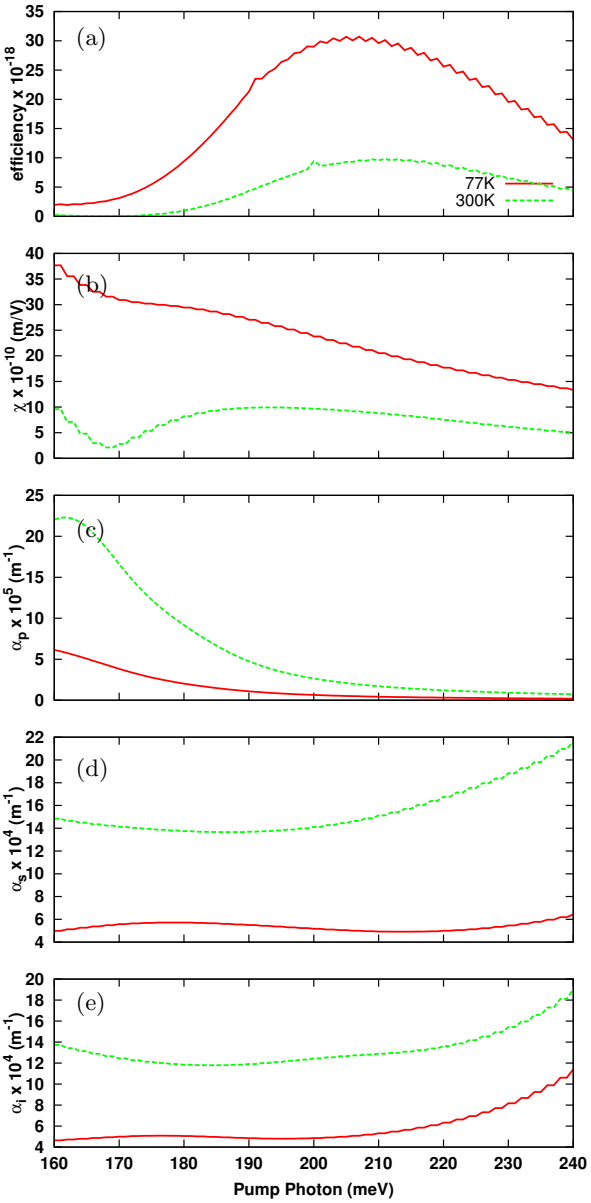

Figure 3: Twin-photon generation efficiency (a), as well as $\chi^{(2)}$ and absorption α (b)-(e), dependence on the pump photon energy, for the interaction length L and hole density fixed to values optimal for the 200 meV pump. The red line in Fig. 3(a) is scaled down by 0.1, so that the green line is also visible in the plot.

References

[1] Gisin N and Thew R 2007 *Nat. Photonics* **1** 165–171
[2] Volz J, Scheucher M, Junge C and Rauschenbeutel A 2014 *Nat. Photonics* **8** 965–970
[3] Barz S 2015 *J. Phys. B: At. Mol. Opt. Phys.* **48** 083001
[4] Ekert A K 1991 *Phys. Rev. Lett.* **67** 661
[5] Bussières F, Clausen C, Tiranov A, Korzh B, Verma V B, Nam S W, Marsili F, Ferrier A, Goldner P, Herrmann H, Silberhorn C, Sohler W, Afzelius M and Nicolas G 2014 *Nat. Photonics* **8** 775–778

[6] Pavičić M 2011 *Int. J. Quantum Inf.* **9** 1737–1744
[7] Sarrafi P, Zhu E Y, Dolgaleva K, Holmes B M, Hutchings D C, Aitchison J S and Qian L 2013 *App. Phys. Lett.* **103** 251115
[8] Klyshko D 1988 *Photons and nonlinear optics* (New York USA: Gordon and Breach)
[9] Xiong C, Marshall G D, Peruzzo A, Lobino M, Clark A S, Choi D Y, Madden S J, Natarajan C M, Tanner M G, Hadfield R H, Dorenbos S N, Zijlstra T, Zwiller V, Thompson M G, Rarity J G, Steel M J, Luther-Davies B, Eggleton B J and O'Brien L 2011 *App. Phys. Lett.* **98** 051101
[10] Di Giuseppe G, Atatüre M, Shaw M D, Sergienko A V, Saleh B E and Teich M C 2002 *Phys. Rev. A* **66** 013801
[11] Young R, Stevenson R, Atkinson P, Cooper K, Ritchie D and Shields A 2006 Entangled photons on-demand from a single quantum dot *Lasers and Electro-Optics, 2006 and 2006 Quantum Electronics and Laser Science Conference. CLEO/QELS 2006. Conference on* pp 1 –2
[12] Chen Y, Zhang J, Zopf M, Jung K, Zhang Y, Keil R, Ding F and Schmidt O G 2016 *Nat. Commun.* **7**
[13] Rao D B, Yang S and Wrachtrup J 2015 *Phys. Rev. B* **92** 081301
[14] Razali R, Valavanis A, Cooper J, Ikonić Z, Indjin D and Harrison P 2016 *Superlattices. Microstruct.* **90** 107–116
[15] Cusack M, Shaw M and Jaros M 1994 *Phys. Rev. B* **49** 16575
[16] Boyd R W 2008 *Nonlinear Optics* (New York USA: Academic Press)
[17] Harrison P 2009 *Quantum wells, wires and dots: theoretical and computational physics of semiconductor nanostructures* (UK: John Wiley & Sons)
[18] Suhara T and Nosaka T 2006 *IEEE J. Quant. Electron.* **42** 777–784
[19] Adachi S 1985 *J. Appl. Phys.* **58** R1–R29
[20] Skauli T, Kuo P, Vodopyanov K, Pinguet T, Levi O, Eyres L, Harris J, Fejer M, Gerard B, Becouarn L and Lallier E 2003 *J. Appl. Phys.* **94** 6447–6455
[21] Suhara T and Kintaka H 2005 *IEEE J. Quant. Electron.* **41** 1203–1212